forests

MDPI

Article

Spatio-Temporal Configurations of Human-Caused Fires in Spain through Point Patterns

Sergi Costafreda-Aumedes [1,*], Carles Comas [2] and Cristina Vega-Garcia [1,3]

1 Department of Agriculture and Forest Engineering, University of Lleida, Alcalde Rovira Roure 191, Lleida 25198, Spain; cvega@eagrof.udl.cat
2 Department of Mathematics, University of Lleida, Agrotecnio Center, Avinguda Estudi General 4, Lleida 25001, Spain; carles.comas@matematica.udl.cat
3 Forest Sciences Centre of Catalonia, Ctra. Sant Llorenç de Morunys km 2, Solsona 25280, Spain
* Correspondence: scaumedes@gmail.com; Tel.: +34-973-702-876

Academic Editors: Yves Bergeron and Sylvie Gauthier
Received: 23 June 2016; Accepted: 18 August 2016; Published: 26 August 2016

Abstract: Human-caused wildfires are often regarded as unpredictable, but usually occur in patterns aggregated over space and time. We analysed the spatio-temporal configuration of 7790 anthropogenic wildfires (2007–2013) in nine study areas distributed throughout Peninsular Spain by using the Ripley's K-function. We also related these aggregation patterns to weather, population density, and landscape structure descriptors of each study area. Our results provide statistical evidence for spatio-temporal structures around a maximum of 4 km and six months. These aggregations lose strength when the spatial and temporal distances increase. At short time lags after a wildfire (<1 month), the probability of another fire occurrence is high at any distance in the range of 0–16 km. When considering larger time lags (up to two years), the probability of fire occurrence is high only at short distances (>3 km). These aggregated patterns vary depending on location in Spain. Wildfires seem to aggregate within fewer days (heat waves) in warm and dry Mediterranean regions than in milder Atlantic areas (bimodal fire season). Wildfires aggregate spatially over shorter distances in diverse, fragmented landscapes with many small and complex patches. Urban interfaces seem to spatially concentrate fire occurrence, while wildland-agriculture interfaces correlate with larger aggregates.

Keywords: inhomogeneous spatio-temporal point patterns; Ripley's K-function; spatio-temporal point patterns; wildfires

1. Introduction

Human-caused fires (HCFs) do not occur randomly, they follow spatio-temporal patterns that change depending on the socioeconomic activity linked to the use or misuse of fire triggering ignitions [1]. Ignition points have been proved to show broadly identifiable spatial and temporal patterns [2]. For instance, fire starts have occurred most often near roads [3], near urban- and cropland-forest interfaces [4] and in areas with an extensive presence of shrubs or conifers [5]. Fire starts also showed clustered temporal structures due to the seasonal distribution of the risk of ignitions [6].

The number of HCFs can vary widely between locations and time spans. Thus, the characterization of spatio-temporal patterns of fire ignition can provide important information for optimizing resource allocation in strategic firefighting [7]. Fire management strategies usually focus on the control of potential multiple-fire situations in areas and periods with high risk of fire [8]. Because of budgetary restrictions and rising firefighting costs, it is usually impossible to maintain sufficient resources to cope with all potential multiple-fire occurrences. In fact, under extreme weather conditions, available firefighting resources may be overloaded beyond suppression capacity. In these cases, the ability to

anticipate high-risk wildfire conditions and take preventive actions, or to pre-position firefighting resources in advance, can reduce the damages and optimize the use of the suppression resources [7,9].

A number of previous studies have focused on the spatial and/or temporal distribution of wildland fires. For instance, [10] identified the most significant spatial variables for analysing human-caused wildfire occurrences using non-spatially explicit models (autoregressive Poisson and logit processes). Other studies have used spatially explicit models to explain patterns of fire occurrence, for instance, geographically weighted regression models [11], ignition density estimates [12], log-Gaussian Cox processes [13,14], scan statistics permutation [15], or Ripley's K-function [16–18]. A few studies have focused on the temporal pattern of fire ignitions; [19] found temporal aggregations using temporal trajectory metrics of wildfire ignition densities, while [20] found temporal aggregations when analysing the fire weather indices of summer fire ignitions in Finland. In addition, time series of the fire occurrence models of [6] included temporal and spatio-temporal lags lasting up to 2–3 days.

Wildfire occurrences have also been analysed as points placed within a spatio-temporal region using point process statistical tools. These tools include, for instance, analysis of inhomogeneous spatio-temporal structures of wildfire ignitions [21], cluster analysis [15,22], modelling of fire locations by spatio-temporal Cox point processes [23], and spatio-temporal analysis of fire ignition points combined with geographical and environmental variables [2]. For instance, [21] analysed space-time configuration of forest fires assuming spatial tools for each year of study separately, and they did not consider a continuous space-time approach for the fire occurrence.

Here we consider inhomogeneous spatio-temporal point processes to analyse the point pattern configuration of human-caused wildfire ignition points of several data sets in Spain. We applied the inhomogeneous spatio-temporal counterpart version of Ripley's K-function proposed by Gabriel & Diggle [24]. This approach was adopted because of the apparent inhomogeneous structure of the spatio-temporal point patterns suggested by the analysis of available official fire reports from the Spanish Ministry of Environment. The analysis of these point configurations would be valuable for interpreting the space-time dependencies of fire ignition points in order to understand wildfire dynamics.

The expected spatial and temporal aggregation patterns of HCFs should be related to the underlying fire risk factors [10] found in previous work such as weather or population. Land use has been used often as a proxy variable for distribution of vegetation/fuels and the presence and activity of human sources of ignition [25,26]. However, the spatial structure of the land mosaic is rarely considered [26], although its composition, configuration, and length of land use interfaces should be of special interest in spatial processes like this. Advances in landscape ecology provide abundant indices to measure mosaic characteristics [27]. Consequently, we also test linear correlations between spatial and temporal parameters derived from the fire patterns and relevant spatial variables linked to the structure of the fire environment with the Pearson product-moment correlation coefficient [28].

2. Materials and Methods

2.1. Study Area

This study analysed nine regions in windows of 40 km × 40 km distributed over forested areas (at least >20% forest area) in Peninsular Spain (Figure 1). These study areas comprise a wide range of forest environments with different landscape structures, but all have fire use levels conducive to significant fire occurrence (at least 100 fires over the study period).

Most of peninsular Spain is dominated by a Mediterranean climate, and only 15% of the land area, located in the north, has an Atlantic climate. These climatic zones and the complex topography combined with human socio-economic development over millennia have given way to a very uneven spatial distribution of the vegetation, combining the presence of medium-scale farming areas, areas with scarce natural vegetation cover (grasses, rangelands), extensive shrub-lands, park-like open forest structures (*dehesas*) with undergrowth, and high forests of variable densities [29]. Tables 1

and 2 include a subset of the total number of independent variables that were generated to capture weather, socioeconomic, and landscape composition and configuration traits of the nine study areas; these variables were selected for their potential relation to the spatio-temporal aggregation of fires. Population density was derived from the municipal registry of 2014 available on the website of the National Institute of Statistics of Spain (http://www.ine.es) and is weighted by the township area included in each study area. Annual climate data was derived from the Digital Climate Atlas of the Iberian Peninsula (1971–2000) (http://www.opengis.uab.es). Landscape ecology indices (landscape and class levels) [27] were calculated with Patch Analyst 5.2 [30] extension of ArcGis 10.3 over a land use reclassification (Figure 2) of the Forest Map of Spain (digitized at 1:50,000 from 1997 to 2006) from Ruiz de la Torre and available on the website of the Spanish Nature Databank of the Ministry of Agriculture, Food and Environment (http://www.magrama.gob.es). Woodland-urban interfaces (WUI), woodland-agriculture interfaces (WAI), and urban-agriculture interfaces (UAI) were evaluated, firstly, calculating a 100 m-buffer of each land use [31] and intersecting them, and secondly, by dividing the area of each interface by all interface areas.

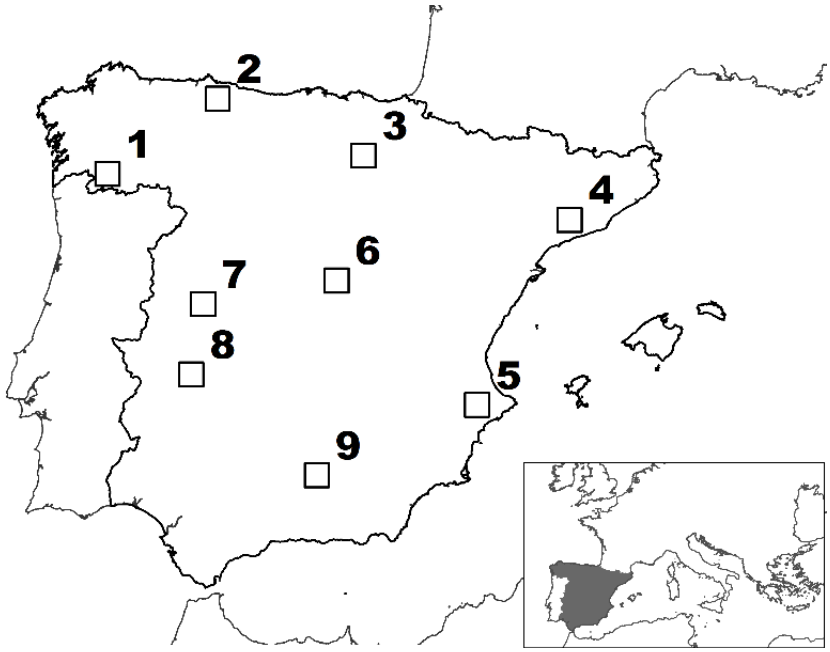

Figure 1. Location of the nine study areas in the Spanish peninsula. 1. Ourense; 2. Asturias; 3. La Rioja; 4. Tarragona; 5. Alicante; 6. Guadalajara; 7. Caceres; 8. Badajoz; 9. Jaen.

Table 1. A subset of independent variables for general characterization of each study area.

Location	*Pp*	Weather		Land Use			Interfaces			Landscape Metrics				
		Tmax	*P*	*Wil*	*Agr*	*Urb*	*WUI*	*WAI*	*UAI*	*NP*	*MdPS*	*MPE*	*PAR*	*SDI*
Ourense	37.1	17.8	1076	67.0	31.5	1.0	4.3	90.4	2.9	493	21.7	16.1	0.37	0.71
Asturias	275.4	16.9	1169	56.1	39.4	4.3	4.7	82.8	10.9	1516	8.8	10.5	0.66	0.84
La Rioja	112.7	17.4	606	36.9	59.9	2.9	4.2	81.9	10.6	4469	0.6	3.1	1.54	0.80
Tarragona	89.9	18.9	583	45.3	50.9	3.7	3	86.6	4.8	1542	6.3	9.2	0.83	0.83
Alicante	135.9	20.3	541	53.6	42.0	4.0	7.5	65.7	12.2	1401	5.3	8.2	0.55	0.85
Guadalajara	298.3	19.6	478	24.5	68.7	6.6	3.8	85.1	9.8	1023	8.2	10.8	0.54	0.79
Caceres	32.7	18.4	1073	81.0	17.5	0.9	3.9	88.7	6.9	782	7.6	8.4	0.43	0.55
Badajoz	29.6	22.3	580	49.1	49.0	1.3	4.4	80	12.3	441	12.7	12	0.31	0.79
Jaen	78.9	20.4	568	40.9	57.2	1.8	3.4	86.2	8.8	966	5.2	7.5	0.54	0.77

Pp: Population density (inhab/km^2); *Tmax*: Annual maximum temperature (°C); *P*: Annual precipitation (mm); *Wil*: Forest, shrubs and pastures (%); *Agr*: Croplands (%); *Urb*: Urban (%); *WUI*: Wildand-Urban interface (%); *WAI*: Wildland-Agriculture interface (%); *UAI*: Urban-Agriculture interface (%); *NP*: Number of patches; *MdPS*: Median patch size (ha); *MPE*: Mean patch edge (km); *PAR*: Perimeter-Area ratio (km/ha); *SDI*: Shannon's diversity index.

Table 2. Landscape ecology metrics at the land use class level by study area.

Location	Land Use	*CA*	*NP*	*MPS*	*MdPS*	*PSSD*	*MPE*	*ED*	*PAR*	*MSI*
Ourense	Agriculture	31.5	316	159.6	28.7	0.705	11.6	23	324.7	2.896
	Wildland	67	127	843.9	11.2	7.136	30.4	24.2	508.3	2.386
	Urban	1	44	37.7	10.6	0.086	6.5	1.8	284.1	2.434
	Water	0.5	6	124.1	25.2	0.207	16	0.6	438.2	4.157
Asturias	Agriculture	39.4	793	79.5	11.2	0.795	9.4	46.8	773.8	3.015
	Wildland	56.1	422	212.6	9.5	2.594	16.7	44	569.9	2.904
	Urban	4.3	289	23.7	3.8	0.216	4.5	8.1	472.3	2.445
	Water	0.2	12	31.8	19.3	0.030	10.6	0.8	412.0	5.084
La Rioja	Agriculture	59.9	1494	64.1	0.8	0.952	4.3	40.2	916.4	1.814
	Wildland	36.9	2302	25.7	0.4	0.668	2.7	38.9	2198.3	2.047
	Urban	2.9	621	7.4	0.9	0.044	16.4	6.4	679.3	1.860
	Water	0.4	52	11.1	1.5	0.030	4.5	1.5	543.8	2.470
Catalonia	Agriculture	50.9	722	112.8	6.4	0.123	9.4	42.6	580.8	2.565
	Wildland	45.3	616	117.7	5.5	2.206	10.6	40.7	1290.5	2.920
	Urban	3.7	199	30.1	9.4	0.079	3.8	4.8	340.1	2.184
	Water	0.1	5	21.0	20	0.012	7.8	0.2	376.6	4.676
Alicante	Agriculture	42	804	83.6	6.5	0.342	6.7	33.9	487.1	2.369
	Wildland	53.6	352	243.8	3.1	4.228	14	30.7	810.5	2.255
	Urban	4	226	28.5	7.1	0.115	4.3	6	345.3	2.219
	Water	0.3	19	29.0	9.8	0.042	9.6	1.2	620.1	5.406
Guadalajara	Agriculture	68.7	388	283.4	8.3	2.251	13.7	33.2	726.3	2.323
	Wildland	24.5	460	85.4	7.1	0.468	10.7	30.8	501.5	2.833
	Urban	6.6	165	64.4	12.1	0.401	4.6	4.7	195.9	1.861
	Water	0.1	10	13.4	11.6	0.009	7.3	0.5	473.7	5.040
Caceres	Agriculture	17.5	493	56.7	9.5	0.201	6.1	18.7	381.4	2.407
	Wildland	81	138	939.2	4.5	10.875	22.9	19.7	745.2	2.153
	Urban	0.9	110	13.1	6.2	0.022	2.4	1.6	268.5	1.962
	Water	0.6	41	24.7	6.6	0.066	4.3	1.1	354.2	2.846
Badajoz	Agriculture	49	202	387.9	13.4	1.409	11.2	14.1	243.8	2.014
	Wildland	49.1	135	582.0	10.9	4.315	15.8	13.4	421.2	2.507
	Urban	1.3	62	34.3	16.4	0.077	8.3	3.2	239.4	2.911
	Water	0.6	42	22.7	12.3	0.042	8.9	2.3	420.7	4.471
Jaen	Agriculture	57.2	298	306.9	5.1	2.659	11.8	21.9	686.2	2.093
	Wildland	40.9	524	124.8	5.3	2.353	6.2	20.3	513.5	2.273
	Urban	1.8	123	23.8	5.5	0.086	3.6	2.7	323.5	2.043
	Water	0.1	21	9.4	4.7	0.025	2.6	0.3	487.3	2.658

CA: Land use class (%); *NP*: Number of patches; *MPS*: Mean patch size (ha); *MdPS*: Median patch size (ha); *PSSD*: Patch size standard deviation (ha); *MPE*: Mean patch edge (km); *ED*: Edge density (km/ha); *PAR*: Perimeter-Area ratio (km/ha); *MSI*: Mean shape index.

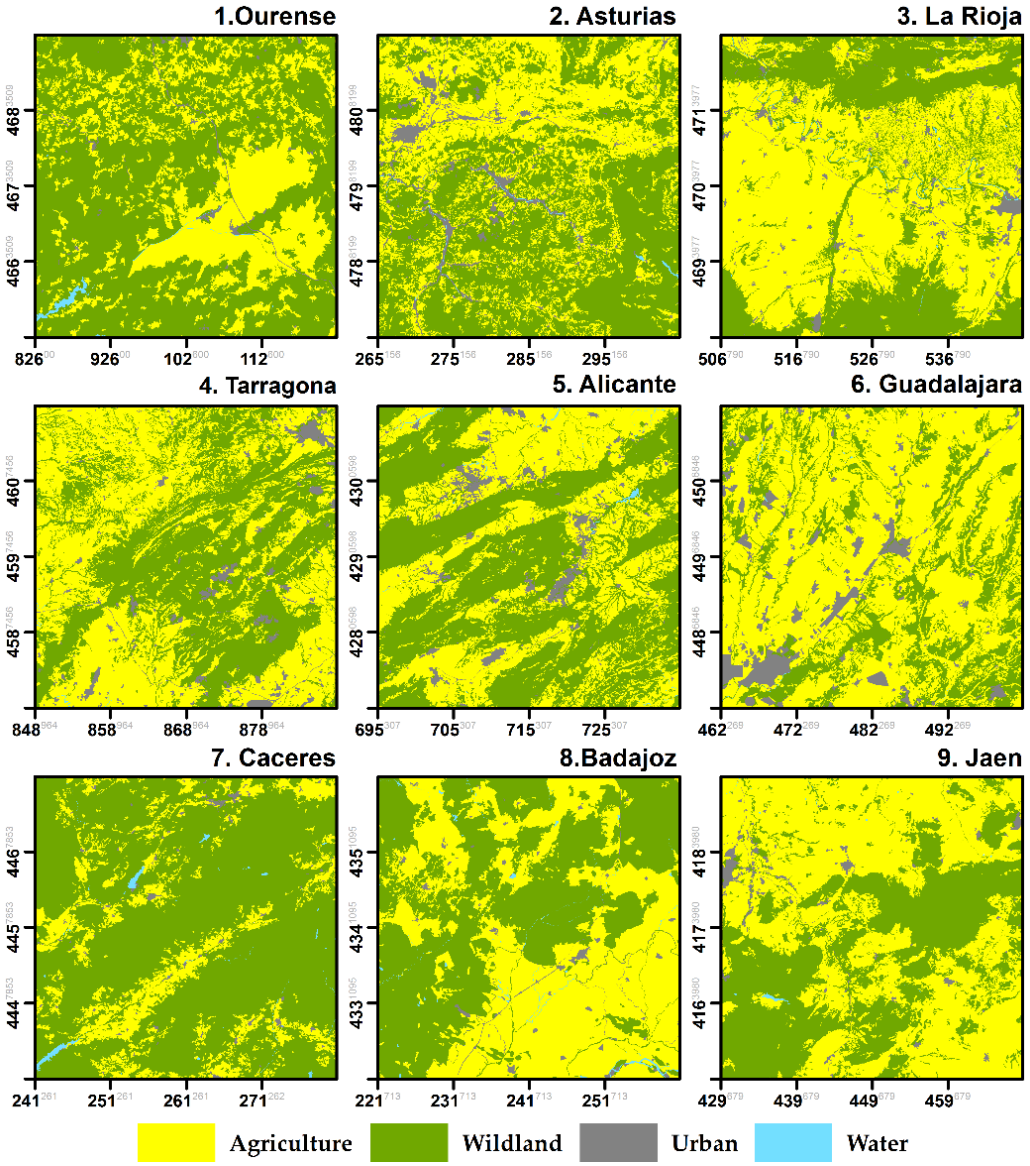

Figure 2. Land use map of the study areas.

2.2. Fire Data

The Spanish Forest Service of the Ministry of Environment and Rural and Marine Affairs (MAGRAMA) provided the fire records for the study. The nine study areas held a sufficient number of fire ignition points to study the spatio-temporal dynamics of fire ignition: at least 100 fires over the study period. Our data sets involved historical records of daily human-caused fire occurrences during the period 2007–2013. The period of study was restricted to seven years due to data availability (precise GPS locations available), but this period was considered appropriate because it surpassed the usual time framework for fire prevention planning in Spain [32]. This period included a variety of weather conditions, with mild years but also years with high risk weather conditions, i.e., 2006 in NW Spain (1900 fires set in just 12 days in August) [33].

The spatio-temporal point pattern analysed consisted of 7790 fire ignition points located in nine square areas of 40 km × 40 km for the seven years, with 877 ignitions in 2007, 1060 in 2008, 1298 in 2009, 1032 in 2010, 1308 in 2011, 1478 in 2012, and 903 in 2013. Figure 3 displays their distribution by study area, monthly.

Figure 4 shows the HCFs spatial pattern of the nine selected study regions. Visual inspection of the point pattern in the nine plots suggests that the point structures are inhomogeneous, with areas of high point intensity juxtaposed to areas of low point intensity. This figure also highlights the presence of point clusters, suggesting that fire events aggregate in space and in time.

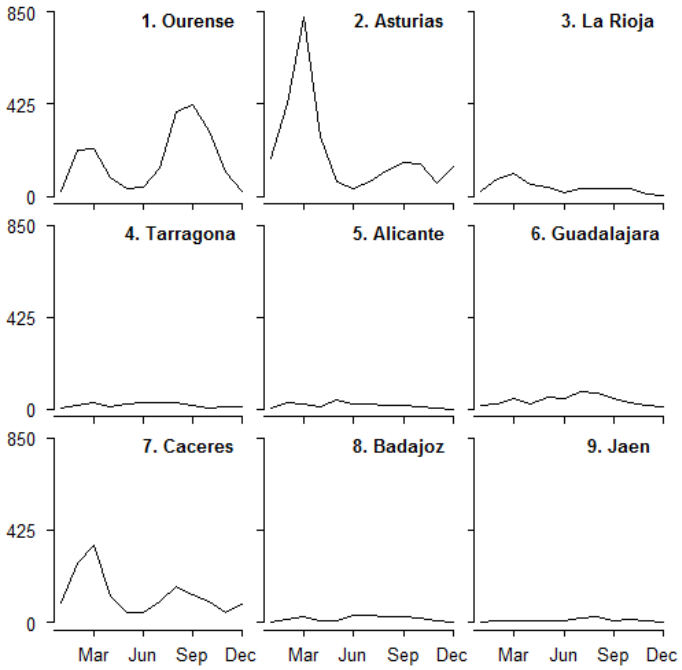

Figure 3. Human-caused wildfire frequency for the period 2007–2013 given by study area and month.

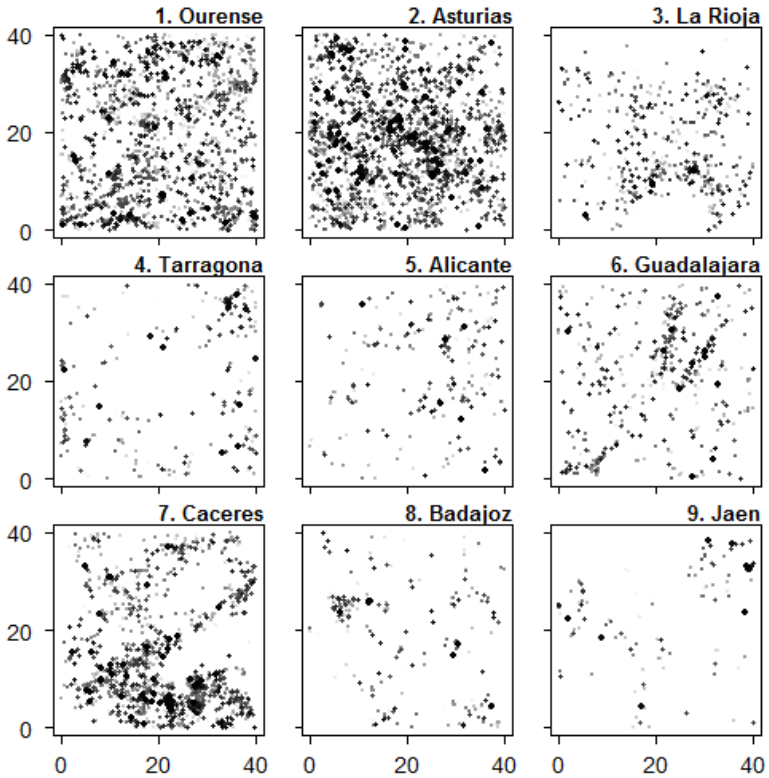

Figure 4. Spatial positions of the 7790 human-caused fires (HCFs) in the study. The biggest and darkest points correspond to recent fires while the lightest points occurred earlier.

2.3. Spatio-Temporal Statistics

To analyse the spatio-temporal structure of inhomogeneous point patterns representing ignition point fires, we used the spatio-temporal counterpart version of Ripley's K-function proposed by [24]. For a review about space-time point processes see [34]. Consider a stationary and anisotropic spatio-temporal point process Φ on $\Re^2 \times \Re$ whose elements form a countable set $S_i = (X_i, t_i)$, for $i = 1, \ldots, n$ and $X_i = (x_i, y_i) \in \Re^2$ and $t_i \in \Re$ in a bounded region $M = W \times T$. This M region contains all the ignition fires for a given planar region W for a time interval $T \in [T_0, T_1]$. Now, the point pattern should be assumed as a set of points in a continuous tridimensional space. The inhomogeneous spatio-temporal Ripley's K-function proposed by [24] assumes that the point pattern under analysis is second-order intensity reweighted stationary and isotropic or, in other words, it assumes a weaker form of stationarity and, therefore, relaxes the hypothesis of homogeneity. A point process is stationary and isotropic if its statistical properties do not change under translation and rotation, respectively. Informally, stationarity implies that one can estimate properties of the process from a single realization on W × T, by exploiting the fact that these properties are the same in different, but geometrically similar, subregions of W × T; isotropy means that there are no directional effects. Function $K_{st}(u, v)$ is the expected number of further points in a spatio-temporal region delimited by a cylinder whose bottom surface area is centred at an arbitrary point of Φ (a point process) with radius u (a spatial distance) and height $2v$ (a time interval). For any inhomogeneous Poisson process (i.e., a Poisson process where the constant intensity is replaced by a spatially varying intensity function) with spatio-temporal intensity function bounded away from zero, $K_{st}(u, v) = 2\pi u^2 v$, and hence $K_{st}(u, v) - 2\pi u^2 v$ (i.e., the empirical spatio-temporal Ripley's K-function minus this function under the hypothesis of no spatial-temporal structure, fire ignitions are independently distributed) can be considered a measure for detecting spatio-temporal point dependences [24]. Values of $K_{st}(u, v) - 2\pi u^2 v < 0$ will indicate regularity, while $K_{st}(u, v) - 2\pi u^2 v > 0$ will suggest spatio-temporal clustering. Moreover, $K_{st}(u, v)$ can also be used to detect the absence of spatio-temporal interaction. In particular, separability of $K_{st}(u, v)$ into purely spatial and temporal components, $K_{st}(u, v) = K_s(u)K_t(v)$, suggests the absence of spatio-temporal dependency [35]. The lack of spatio-temporal interaction indicates that ignition point locations and ignition times are independent, i.e., there is no correlation between where a fire happens and when it happens. However, in real life one may expect these two components to be correlated, so the time occurrence of a fire will depend on the spatial location. An edge-corrected estimator of $K_{st}(u, v)$ can be defined via [36].

$$\hat{K}_{st}(u, v) = \frac{1}{|W \times T|} \sum_{i=1}^{n} \sum_{j \neq i}^{n} \frac{1}{\omega_{ij} v_{ij}} \frac{I(u_{ij} \leq u) I(|t_j - t_i| \leq v)}{\hat{\lambda}(S_i)\hat{\lambda}(S_j)} \quad (1)$$

where n is the total number of points in M, $u_{ij} = \| X_i - X_j \|$, $I(\cdot)$ is the indicator function where $I(F) = 1$ if F is true and $I(F) = 0$ otherwise, $|W \times T|$ denotes the volume of this region and $\hat{\lambda}(\cdot)$ is an estimator of the spatio-temporal intensity function at the location S_i or, in other words, an estimator of expected number of points per unit volume at this exact location. To correct spatial edge effects we use Ripley's factor ω_{ij} [37] and to deal with time-edge effects we consider v_{ij}. This v_{ij} equals 1 if both ends of the interval of length $2|t_j - t_i|$ centred at t_j lie between T, and it equals 1/2 otherwise [36]. Note that correctors for edge-effects are necessary to deal with window sampling where information outside this space-time window (unobserved points) is lost, introducing, usually, a negative bias for $\hat{K}_{st}(u, v)$. Edge-effect correctors such as the Ripley's factor and the time correction considered here are standard approximations to reduce these bias effects based on mathematical arguments. Usually these arguments consider that the unobserved numbers of points outside the observation windows are proportional to those inside these windows.

In order to obtain (1), we need to obtain an estimator of the spatio-temporal intensity function. Here we adopted a kernel-based estimator for this space-time function. First we need to assume

that first-order effects (i.e., the intensity function) are separable from the space and the time domain, as suggested by Gabriel & Diggle [24], i.e.,

$$\lambda(X,t) = m(X)\mu(t) \tag{2}$$

and thus any non-separable effects can be considered as second-order effects (i.e., related to the variance of the process) rather than first-order effects. Then from Equation (2) we can estimate $\lambda(\cdot)$ [38] as:

$$\hat{\lambda}(X,t) = \hat{m}(X)\hat{\mu}(t)/n \tag{3}$$

as:

$$\int_W \hat{m}\,(X)d\,(X) = \int_T \hat{\mu}\,(t)d\,(t) = n \tag{4}$$

Now, we can estimate both the space and the time intensity function separately. For the space point intensity $m(X)$, we used a Gaussian kernel-based estimator, with bandwidth initially chosen to minimize the estimated mean-square error of $\hat{m}(X)$, as suggested in [39]. In some cases, this optimal bandwidth was slightly increased to provide a good visual fitting to the point patterns. Moreover, for time point intensity, we adopted a Gaussian kernel estimator since we did not consider covariate information related the fire locations.

Note that a kernel-based estimator for the time intensity does not assume any previous knowledge of the time series, while providing a reasonable approximation for the intensity function. After some experimentation, we considered $\sigma_\mu = 10.0$ as it provides a good visual fitting to the data while reproducing quite well some of the outliers observed in the time series.

To test for evidence of spatio-temporal clustering or regular structures, we compared the estimator $\hat{K}_{st}(u,v)$ with estimates obtained for simulations under a suitable null hypothesis. Here the null hypothesis is that the underlying point process is an inhomogeneous Poisson process, and, therefore, the empirical spatio-temporal pattern is compared with a spatio-temporal Poisson process with point intensity (3) based on a Monte Carlo test. This is a space-time Poisson process where the constant intensity is replaced by a spatially varying intensity function estimated by (3).

We simulated 1000 spatio-temporal point patterns under this null hypothesis and for each one an estimator of Equation (1) was obtained. This set of functions was then compared with the resulting estimator for the empirical data under analysis. Under this test, we rejected the null hypothesis (spatio-temporal point independence) if the resulting estimator of this function lay above the 95th percentile of estimates calculated from the 1000 simulations of inhomogeneous Poisson point process with intensity (3). This 95th percentile of estimated values formed the tolerance envelopes for our test. In this case, we should accept spatio-temporal clustering of fire locations.

All the spatio-temporal statistical analyses were computed using the stpp statistical package [36] for the R statistical environment [40].

2.4. Spatio-Temporal Aggregation Trends

In order to explain possible spatio-temporal HCFs aggregations, the Pearson product-moment correlation coefficient was selected to measure the strength of the linear dependence between the spatial and temporal aggregation patterns of HCFs and the independent weather, socioeconomic, and landscape composition and configuration variables (Tables 1 and 2). This estimator ranges from +1 to -1, where the positive and negative values indicate, respectively, positive and negative correlation (data-pairs best regression fit), and 0 indicates no significant correlation between variables [12].

3. Results

3.1. Spatio-Temporal Aggregation of HCFs

In Figure 5, we compare $\hat{K}_{st}(u,v) - 2\pi u^2 v$ and tolerance envelopes suggesting the presence of different spatio-temporal structures for time lags of less than two years and ignition point distances in the range of 0–16 km. In particular, this figure provides results on clustering patterns in the nine regions under analysis; black values indicate spatio-temporal clustering for these space-time scales. We used these maximum time and space intervals to avoid edge effects that may not be corrected by the mathematical assumptions made here. The maximum scale of the spatio-temporal aggregation of HCFs was found to be around 4–4.5 km and 5.5–6 months in Tarragona, and the minimum, less than one month and one km, in La Rioja. The spatio-temporal structures generally lose strength as the time lag increases; at the time lag of six months or higher, these dependencies are only observable for short inter-ignition point distances of less than 3 km.

However, in the NW of Spain with Atlantic climate (Ourense and Asturias), the spatial pattern shows a cyclical aggregation trend of around one year (a hump in the plot around the 12-month value). These Atlantic areas also display aggregation up to the maximum spatial distance considered (16 km) for all time lags under three months. This means that once a fire happens, the probability that another takes place within a wide area around the first one (up to 16 km in radius) persists for a period close to three months. In the other study areas, the probability that an additional fire occurs once one takes place, only persist for the maximum distance (up to 16 km in radius) for short time lags (less than 1–2 months).

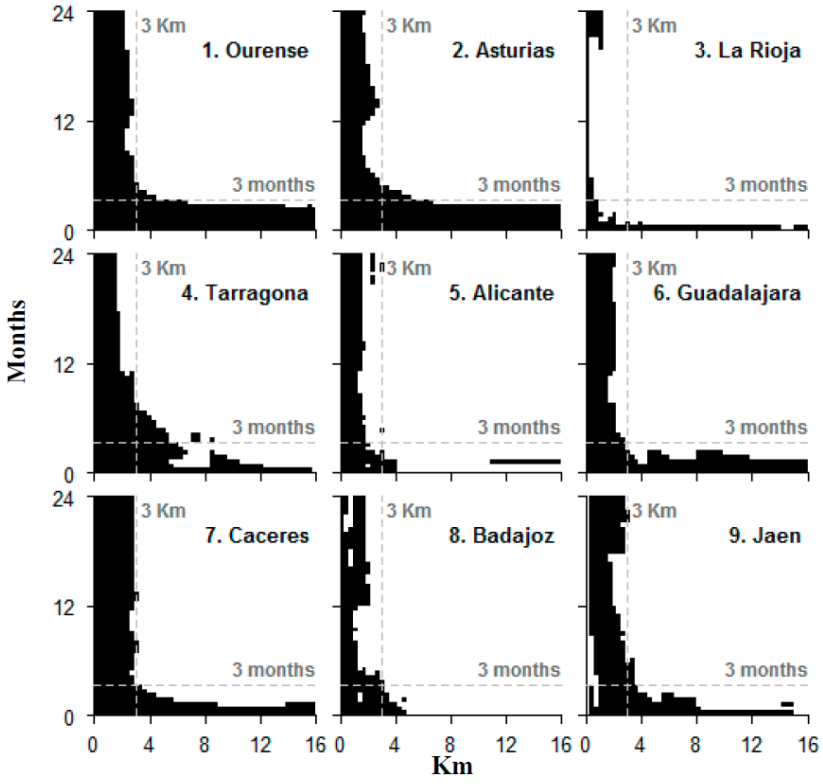

Figure 5. Comparison between $\hat{K}_{st}(u,v) - 2\pi u^2 v$ and tolerance envelopes indicating spatio-temporal clustering (black values) for each study area. Reference of 3 km and three months in grey dotted line.

3.2. Trends of the Spatio-Temporal HCFs Pattern

The values found in each plot at the limits of the maximum intervals considered or axis—the x for 24 months, $x24$; the y for 16 km, $y16$—were taken as descriptors of spatial and temporal aggregation.

$x24$ is the spatial lag for aggregation at any time lag (spatial lag of aggregation independent of the time lag). $y16$ is the time lag for aggregation at any spatial lag considered (time lag of aggregation independent of the space lag). Table 3 shows the Pearson's correlation between those aggregation parameters, the number of fires of Figure 3 and the descriptive variables of Table 1 at the landscape level. The number of HCFs shows a positive correlation with the time-independent spatial aggregation values $x24$, even higher with the distance-independent temporal aggregation values $y16$. Therefore, the higher the fire occurrence caused by humans, the more likely fires aggregate over longer distances and longer time frames, and vice versa.

Table 3. Pearson product-moment correlation coefficient between each variable of Table 1 and the descriptors of spatial and temporal aggregation. In bold, values over 0.5.

Variable	Spatial $x24$	Temporal $y16$	Variable	Spatial $x24$	Temporal $y16$
FF	**0.609**	**0.813**	*WAI*	**0.539**	0.192
Pp	−0.218	0.391	*UAI*	**−0.562**	−0.418
Tmax	−0.123	**−0.688**	*NP*	**−0.768**	−0.162
P	**0.696**	**0.693**	*MdPS*	**0.648**	0.488
Wil	**0.683**	0.327	*MPE*	**0.649**	**0.514**
Agr	**−0.681**	−0.371	*PAR*	**−0.744**	−0.157
Urb	−0.422	0.198	*SDI*	**−0.627**	0.035
WUI	−0.221	0.154			

FF: Fire frequency; *Pp*: Population density (inhab/km^2); *Tmax*: Annual maximum temperature (°C); *P*: Annual precipitation (mm); *Wil*: Forest, shrubs and pastures (%); *Agr*: Croplands (%); *Urb*: Urban (%); *WUI*: Wildand-Urban interface (%); *WAI*: Wildland-Agriculture interface (%); *UAI*: Urban-Agriculture interface (%); *NP*: Number of patches; *MdPS*: Median patch size (ha); *MPE*: Mean patch edge (km); *PAR*: Perimeter-Area ratio (km/ha); *SDI*: Shannon's diversity index.

According to the results, higher population density causes distance-aggregation or spatially closer fires and dilates the time lag for wildfire occurrence, but the correlation is not high. Drought weather conditions (higher *Tmax* and lower *P*) influence wildfire aggregates by decreasing the distance and time lags. Weather, mean patch edge (*MPE*), and fire frequency (*FF*, the occurrence of other fires) seem to be the variables mainly related to temporal aggregation of fires.

Proportions of land covers (*Wil*, *Agr*, *Urb*) indicate an effect on spatial aggregation of fires, linked by larger distances in landscapes with higher wildland cover and closer distances in landscapes with a higher relative proportion of agriculture and urban areas. Interfaces between land covers are correlated to the time-independent spatial aggregation of fires, particularly, urban interfaces (*WUI* and *UAI*) seem to spatially concentrate fire occurrence, while *WAI* correlates with larger aggregates.

The time-independent spatial lag for aggregation $x24$ is clearly influenced by landscape composition and configuration, being negatively correlated to *SDI*, *NP* and *PAR* and positively to *MPE* and *MdPS*. In other words, wildfires aggregate over closer distances in diverse, fragmented landscapes with many patches, where patches are small and with complex shapes.

Table 4 shows the Pearson's correlation between the descriptors of spatial and temporal aggregation and the variables in Table 2 for landscape structure analysed at the land use class level. Higher relative proportion of wildland organized in larger patches (*MPS*, *MdPS*), with more edges (*MPE*), and lower complexity (*PAR*) and number of patches (*NP*) favour larger spatial aggregation distances. In general, fire spatial aggregates grow in coarse-grained landscapes, with decreasing number of patches (*NP*) and compact shapes (*PAR*) in all land use classes. The temporal lag for aggregation of fires seems to be positively related to the presence of larger and complex agriculture patches (*MdPS*, *MSI*), and wildland edges (*MPE*).

Table 4. Pearson product-moment correlation coefficient between each variable in Table 2 with the descriptors of spatial and temporal aggregation. In bold, values over 0.5.

	Class	*NP*	*MPS*	*MdPS*	*PSSD*	*MPE*	*ED*	*PAR*	*MSI*
Spatial *x*24	*Agr*	**−0.696**	0.042	**0.659**	−0.108	0.378	−0.444	**−0.521**	**0.635**
	Wil	**−0.769**	**0.711**	**0.580**	**0.709**	**0.777**	−0.403	**−0.712**	0.109
	Urb	**−0.761**	0.107	0.200	−0.054	0.245	**−0.597**	**−0.575**	0.204
Temporal *y*16	*Agr*	0.009	−0.459	**0.572**	−0.344	0.161	0.421	0.073	**0.915**
	Wil	−0.257	0.163	0.389	0.145	**0.569**	0.459	−0.241	0.364
	Urb	−0.089	0.174	−0.200	0.304	0.062	0.227	0.040	0.044

Wil: Forest, shrubs and pastures (%); *Agr*: Croplands (%); *Urb*: Urban (%); *NP*: Number of patches; *MPS*: Mean patch size (ha); *MdPS*: Median patch size (ha); *PSSD*: Patch size standard deviation (ha); *MPE*: Mean patch edge (km); *ED*: Edge density (km/ha); *PAR*: Perimeter-Area ratio (km/ha); *MSI*: Mean shape index.

4. Discussion

The methodology used appears to be suitable for identifying differentiated patterns of spatio-temporal aggregation for HCFs in environments with different fire incidence, such as Peninsular Spain, even though the influence of window size (40 km × 40 km) and study period remains to be explored in future research. This method is especially useful in regions with enough observations because its negative simulations' bias decreases as the number of observations increases [24]. The largest spatial and temporal distances for wildfire aggregation were found with increased fire occurrence, which is coherent with higher risk levels that cause more fires over longer time spans and greater distances (i.e., Galicia, Asturias).

Our results provide statistical evidence for spatio-temporal structures around a maximum of 4 km and three months, but these aggregated structures lose strength when the spatial and temporal distances increase. These results agree with previous work [2,17,22,41–43] which detected spatial and temporal structures in wildfire occurrence in Portugal and Spain, and the general state-of-knowledge on fire occurrence in Spain; at short time lags after a wildfire (<1 month), the probability of another fire occurrence is high at any distance in the range of 0–16 km. This is in agreement with the fact that in the short term, weather is the main driver of fire occurrence, and its effects are regional. When considering larger time lags (up to two years, or 24 months), the probability of fire occurrence is high only at short distances, closer than 3 km, which is consistent with the presence of local structural risk factors independent of the season or weather condition (i.e., arson, [13]). These results agree with [15,22], which mention that aggregations between fires are more often at the local level and are not visible in larger distances (15 or 50 km).

Nevertheless, these aggregated patterns vary depending on location in Spain, suggesting the existence of varied spatio-temporal aggregation patterns of HCFs throughout the country, mainly related to fire frequency, weather, and landscape structure variables, and hence, fire regimes.

Patterns in Atlantic (Ourense, Asturias) and Mediterranean Spain (the other areas) differ, which should be expected given their climatic and landscape structure characteristics that determine different fire regimes [5]. The spatial aggregation found (up to the maximum distance considered, 16 km) for all time lags under three months is likely determined by the duration of the bimodal fire season in the milder Atlantic region (February–April, June–August, three months), but also a consequence of a fragmented landscape and a generally high human risk and occurrence all year round. This pattern has also been identified in Portugal [42] linked with the annual cycle of weather and vegetation phenology. Relatively stable conditions with higher rainfall (>1000 mm) and lower maximum temperatures extend risk over longer periods than in the Mediterranean (around 550 mm). Variations of weather events occur gradually in the NW, so the range of variation in temperature and precipitation is low within each Atlantic study area. In areas with higher precipitation there are more rainy days and, therefore, the number of fire-days decreases [44,45], so fires aggregate over longer time lags [24].

Wildfires seem to aggregate within fewer days in warm and dry Mediterranean regions (0–1.5 months). The annual weather cycle [46] favours multiple fires per day or in a few days in the summer fire season [47]. Fire suppression resources sufficient to manage one fire may be challenged on high temperature days with simultaneous occurrences [48], which require exhaustive firefighting personnel management [49]. During high temperature days, the temporal aggregation of HCFs decreases, since the occurrence of new fires is associated to those spells of extreme weather conditions [10,46,50]. Our temporal results are coherent with the occurrence of heat waves (high-temperature days (HTDs) [46]) that combine with more uneven human risk levels over coarser landscapes to render a lower fire occurrence, though these fires may have catastrophic results in terms of burned area.

Previous studies done in the Iberian Peninsula [43,50], found direct relations between population density and HCF occurrence; we found that higher population density causes distance-aggregation or spatially closer fires and dilates the time lag for wildfire occurrence, though the correlations were not very high. We used a single population density value for each study area (40 km $\times$ 40 km), but considering mean distances to towns [3,10,13], access by road [3,51,52], and trails [43,53] could also be adequate to account for the combined effect of population and access on HCF spatio-temporal aggregation.

Landscape structure clearly influences spatio-temporal patterns in wildfire occurrence. We found that wildfires aggregate spatially in closer distances in diverse, fragmented landscapes with many patches, where patches are small and have complex shapes. Ignitions have been found before to concentrate in highly fragmented landscapes [4,54] or, in other words, in areas with a larger number of small patches [25,26] in anthropic environments where patches are more compact [25,26] with shorter edges [19], raising doubts about the role of patch shape on ignition. We propose that patch shape is relevant in combination with landscape composition, depending on the class under consideration and its dominance in the landscape. Landscapes with a higher relative proportion of wildland coverage organized in larger patches (*MPS*, *MdPS*), with more edges (*MPE*), and lower complexity (*PAR*) and number of patches (*NP*) favour larger spatial aggregation distances. In general, fire spatial aggregates cover larger distances in coarse-grained landscapes, with decreasing number of patches (*NP*) and compact shapes (*PAR*) in all classes. These forest landscapes are typically created by land abandonment processes [55] which have been expanding in all the Southern European Mediterranean countries for the last 60 years.

Landscape composition and patch shapes determine the presence of interfaces between land use classes. Urban interfaces with wildlands and crops (*WUI* and *UAI*) seem to spatially decrease the distance for fire clustering, while increasing percentages of wildland-agriculture interfaces correlate with larger aggregates, effectively showing a spatial extension in risk. Previous studies in HCF prediction [43,56] have linked wildfires to agricultural cover over wildland [13,45,51] and urban covers [57]. Fires in Spain often occur at the wildland-agriculture interface [52]. The study areas with a lower proportion of wildland-agriculture interface have wildfires clustered at shorter distances and they seem to aggregate on patch perimeters between these classes (*WAI*). This finding agrees with [57,58] who have also associated a higher proportion of wildland-agriculture interface with an increase of fire occurrence in Spain. Interestingly, the temporal lag for aggregation of fires seems to be positively related to the presence of larger and complex agriculture patches (*MdPS*, *MSI*), and wildland edges (*MPE*) pointing again to the importance of *WAI* interfaces in fire occurrence.

Beyond supporting previous findings in the field of fire occurrence prediction related to fire frequency, weather, and landscape structure variables, we would like to point out that our analysis contributes additional information that is useful for fire management. The descriptors of spatial and temporal aggregation ($x24$, $y16$) have different values in different study areas, and may serve as indicators for diverse applications, for instance, fire regimes classification concerning fire occurrence. A better knowledge of factors related to occurrence is useful for prevention and suppression, but the spatial and temporal dimensions added for each window of analysis have direct operational applications. Wildfire suppression performance in the fire season depends on the number and

behaviour of active fires [49]; fire managers must make crucial decisions on the amount, type, and allocation of the fire suppression resources required. For instance, risk levels and probability of new fire occurrences remain high in Ourense for up to three months, which allows for less mobility in the positioning of initial attack crews than in Badajoz with no temporal aggregation, or La Rioja (<1 month). Spatial risk at any time lag occurs under 0.75 km distance in La Rioja, but reaches 2.75 km in Caceres or Ourense, with implications for the design of the detection network. This persistent local risk is related to complex socioeconomic factors [6], but can be linked to landscape structure, which can also be used to inform general prevention and land planning to avoid risky structures.

5. Conclusions

This study demonstrates the existence of spatio-temporal aggregation patterns of human-caused fires in Peninsular Spain. This aggregation reaches maximum values around 4 km and six months, but decreases with increasing temporal and spatial distances, and varies in different study areas. The probability of an additional fire is higher at any distance in the range of 0–16 km for short periods after a fire. In the long term, the probability of fire occurrence is higher at distances closer than 3 km from the location of a first fire. Temporal aggregation is mainly related to meteorology (annual rainfall and maximum temperature), while spatial aggregation is mainly linked to the structure and composition of the landscape. Our results suggest that wildfires temporally aggregate in fewer days in warm and dry Mediterranean regions than in milder Atlantic areas; wildfires spatially aggregate in fewer kilometres in highly fragmented wildland and agriculture landscapes with high land use diversity, and spatially disperse comparatively more in forest coarse-grained landscapes resulting from abandonment. Our results also suggest the existence of local risk conditions that persist over time, probably related to land structure and complex socioeconomic factors.

Acknowledgments: We gratefully acknowledge the Spanish Ministry of Environment, Rural and Marine Affairs (MAGRAMA) for allowing us to use the historical wildfire registry (EGIF).

Author Contributions: S. Costafreda-Aumedes, C. Comas and C. Vega-Garcia conceived and designed the experiments; C. Comas performed the experiments; S.Costafreda-Aumedes and C. Vega-Garcia analysed the data; S. Costafreda-Aumedes, C. Comas and C. Vega-Garcia wrote the paper.

Conflicts of Interest: The authors declare no conflict of interest.

References

1. González-Olabarria, J.R.; Mola-Yudego, B.; Coll, L. Different Factors for Different Causes: Analysis of the Spatial Aggregations of Fire Ignitions in Catalonia (Spain). *Risk Anal.* **2015**, *35*, 1197–1209. [CrossRef] [PubMed]
2. Juan, P.; Mateu, J.; Saez, M. Pinpointing spatio-temporal interactions in wildfire patterns. *Stoch. Environ. Res. Risk Assess.* **2012**, *26*, 1131–1150. [CrossRef]
3. Badia-Perpinyà, A.; Pallares-Barbera, M. Spatial distribution of ignitions in Mediterranean periurban and rural areas: The case of Catalonia. *Int. J. Wildland Fire* **2006**, *15*, 187–196. [CrossRef]
4. Martínez, J.; Vega-Garcia, C.; Chuvieco, E. Human-caused wildfire risk rating for prevention planning in Spain. *J. Environ. Manag.* **2009**, *90*, 1241–1252. [CrossRef] [PubMed]
5. Verdú, F.; Salas, J.; Vega-García, C. A multivariate analysis of biophysical factors and forest fires in Spain, 1991–2005. *Int. J. Wildland Fire* **2012**, *21*, 498–509. [CrossRef]
6. Prestemon, J.P.; Chas-Amil, M.L.; Touza, J.M.; Goodrick, S.L. Forecasting intentional wildfires using temporal and spatiotemporal autocorrelations. *Int. J. Wildland Fire* **2012**, *21*, 743–754. [CrossRef]
7. Genton, M.G.; Butry, D.T.; Gumpertz, M.L.; Prestemon, J.P. Spatio-temporal analysis of wildfire ignitions in the St Johns River Water Management District, Florida. *Int. J. Wildland Fire* **2006**, *15*, 87–97. [CrossRef]
8. Gonzalez-Olabarria, J.R.; Brotons, L.; Gritten, D.; Tudela, A.; Teres, J.A. Identifying location and causality of fire ignition hotspots in a Mediterranean region. *Int. J. Wildland Fire* **2012**, *21*, 905–914. [CrossRef]
9. Boychuk, D.; Martell, D.L. A Markov chain model for evaluating seasonal forest fire fighter requirements. *For. Sci.* **1988**, *34*, 647–661.

10. Padilla, M.; Vega-Garcia, C. On the comparative importance of fire danger rating indices and their integration with spatial and temporal variables for predicting daily human-caused fire occurrences in Spain. *Int. J. Wildland Fire* **2011**, *20*, 46–58. [CrossRef]
11. De la Riva, J.; Pérez-Cabello, F.; Lana-Renault, N.; Koutsias, N. Mapping wildfire occurrence at regional scale. *Remote Sens. Environ.* **2004**, *92*, 363–369. [CrossRef]
12. Amatulli, G.; Peréz-Cabello, F.; de la Riva, J. Mapping lightning/human-caused wildfires occurrence under ignition point location uncertainty. *Ecol. Model.* **2007**, *200*, 321–333. [CrossRef]
13. Serra, L.; Saez, M.; Mateu, J.; Varga, D.; Juan, P.; Díaz-Ávalos, C.; Rue, H. Spatio-temporal log-Gaussian Cox processes for modelling wildfire occurrence: The case of Catalonia, 1994–2008. *Environ. Ecol. Stat.* **2014**, 531–563. [CrossRef]
14. Najafabadi, A.T.P.; Gorgani, F.; Najafabadi, M.O. Modeling forest fires in Mazandaran Province, Iran. *J. For. Res.* **2015**, *26*, 851–858. [CrossRef]
15. Vega Orozco, C.; Tonini, M.; Conedera, M.; Kanveski, M. Cluster recognition in spatial-temporal sequences: the case of forest fires. *Geoinformatica* **2012**, *16*, 653–673. [CrossRef]
16. Serra, L.; Juan, P.; Varga, D.; Mateu, J.; Saez, M. Spatial pattern modelling of wildfires in Catalonia, Spain 2004–2008. *Environ. Model. Softw.* **2013**, *40*, 235–244. [CrossRef]
17. Fuentes-Santos, I.; Marey-Pérez, M.F.; González-Manteiga, W. Forest fire spatial pattern analysis in Galicia (NW Spain). *J. Environ. Manag.* **2013**, *128*, 30–42. [CrossRef] [PubMed]
18. Turner, R. Point patterns of forest fire locations. *Environ. Ecol. Stat.* **2009**, *16*, 197–223. [CrossRef]
19. Gralewicz, N.J.; Nelson, T.A.; Wulder, M.A. Spatial and temporal patterns of wildfire ignitions in Canada from 1980 to 2006. *Int. J. Wildland Fire* **2012**, *21*, 230–242. [CrossRef]
20. Tanskanen, H.; Venäläinen, A. The relationship between fire activity and fire weather indices at different stages of the growing season in Finland. *Boreal Environ. Res.* **2008**, *13*, 285–302.
21. Hering, A.S.; Bell, C.L.; Genton, M.G. Modeling spatio-temporal wildfire ignition point patterns. *Environ. Ecol. Stat.* **2009**, *16*, 225–250. [CrossRef]
22. Pereira, M.G.; Caramelo, L.; Orozco, C.V.; Costa, R.; Tonini, M. Space-time clustering analysis performance of an aggregated dataset: The case of wildfires in Portugal. *Environ. Model. Softw.* **2015**, *72*, 239–249. [CrossRef]
23. Møller, J.; Díaz-Avalos, C. Structured Spatio-Temporal Shot-Noise Cox Point Process Models, with a View to Modelling Forest Fires. *Scand. J. Stat.* **2010**, *37*, 2–25. [CrossRef]
24. Gabriel, E.; Diggle, P.J. Second-order analysis of inhomogeneous spatio-temporal point process data. *Stat. Neerl.* **2009**, *63*, 43–51. [CrossRef]
25. Henry, M.; Yool, S. Assessing Relationships between Forest Spatial Patterns and Fire History with Fusion of Optical and Microwave Remote Sensing. *Geocarto Int.* **2004**, *19*, 25–37. [CrossRef]
26. Costafreda-Aumedes, S.; Garcia-Martin, A.; Vega-Garcia, C. The relationship between landscape patterns and human-caused fire occurrence in Spain. *For. Syst.* **2013**, *22*, 71–81. [CrossRef]
27. McGarigal, K.; Cushman, S.A.; Ene, E. FRAGSTATS v4: Spatial Pattern Analysis Program for Categorical and Continuous Maps. Computer Software Program Produced by the Authors at the University of Massachusetts, Amherst. Available online: http://www.umass.edu/landeco/research/fragstats.html (accessed on 11 January 2016).
28. Pearson, K. Notes on the History of Correlation. *Biometrika* **1920**, *13*, 25–45. [CrossRef]
29. EEA (European Environment Agency). *European Forest Types. Categories and Types for Sustainable Forest Management Reporting and Policy*; EEA: Copenhagen, Denmark, 2006.
30. Rempel, R.S.; Kaukinen, D.; Carr, A.P. *Patch Analyst and Patch Grid*; Ontario Ministry of Natural Resources Centre for Northern Forest Ecosystem Research: Thunder Bay, ON, Canada, 2012.
31. Ruiz Cejudo, J.A.; Madrigal Olmo, J. Caracterización de la interfaz-urbano forestal en la provincia de Valencia: implicaciones en la evaluación riesgo y en la prevención de incendios forestales. In Proceedings of the 6° Congreso Forestal Español; Vitoria-Gasteiz, España, 10–14 June 2013; p. 16.
32. Generalitat Valenciana. Conselleria de governació i justicia. Plan de prevención de incendios forestales de la demarcación de Altea. In *Instrucciones para la Redacción de Planes de Prevención de Incendios Forestales en Espacios Naturales Protegidos Distintos de Parques Naturales*; Generalitat Valenciana: Valencia, Spain, 2012.
33. Chas-Amil, M.L.; Touza, J.; Prestemon, J.P. Spatial distribution of human-caused forest fires in Galicia (NW Spain). *Ecol. Environ.* **2010**, *137*, 247–258.
34. Illian, J.; Penttinen, A.; Stoyan, H.; Stoyan, D. *Statistical Analysis and Modelling of Spatial Point Patterns*; John Wiley & Sons, Ltd.: Chichester, UK, 2008.

35. Diggle, P.; Chetwynd, A.G.; Häggkvist, R.; Morris, S.E. Second-order analysis of space-time clustering. *Stat. Methods Med. Res.* **1995**, *4*, 124–136. [CrossRef] [PubMed]
36. Gabriel, E.; Rowlingson, B.; Diggle, P.J. Stpp: An R Package for Plotting, Simulating and Analysing Spatio-Temporal Point Patterns. *J. Stat. Softw.* **2013**, *53*, 1–29. [CrossRef]
37. Ripley, B.D. The Second-Order Analysis of Stationary Point Processes. *J. Appl. Probab.* **1976**, *13*, 255–266. [CrossRef]
38. Ghorbani, M. Testing the weak stationarity of a spatio-temporal point process. *Stoch. Environ. Res. Risk Assess.* **2013**, *27*, 517–524. [CrossRef]
39. Berman, M.; Diggle, P. Estimating Weighted Integrals of the Second-Order Intensity of a Spatial Point Process. *J. R. Stat. Soc. Ser. B* **1989**, *51*, 81–92.
40. R Development Core Team. *R: A Language and Environment for Statistical Computing*; The R Core Team: Auckland, New Zealand, UK, 2005; Volume 1.
41. Alonso-Betanzos, A.; Fontenla-Romero, O.; Guijarro-Berdiñas, B.; Hernández-Pereira, E.; Paz Andrade, M.I.; Iménez, E.; Legido Soto, J.L.; Carballas, T. An intelligent system for forest fire risk prediction and fire fighting management in Galicia. *Expert Syst. Appl.* **2003**, *25*, 545–554. [CrossRef]
42. Telesca, L.; Pereira, M.G. Time-clustering investigation of fire temporal fluctuations in Portugal. *Nat. Hazards Earth Syst. Sci.* **2010**, *10*, 661–666. [CrossRef]
43. Chas-Amil, M.L.; Prestemon, J.P.; Mcclean, C.J.; Touza, J. Human-ignited wild fire patterns and responses to policy shifts. *Appl. Geogr.* **2015**, *56*, 164–176. [CrossRef]
44. Boubeta, M.; Lombardía, M.J.; Marey-Pérez, M.F.; Morales, D. Prediction of forest fires occurrences with area-level Poisson mixed models. *J. Environ. Manag.* **2015**, *154*, 151–158. [CrossRef] [PubMed]
45. Garcia-Gonzalo, J.; Zubizarreta-Gerendiain, A.; Ricardo, A.; Marques, S.; Botequim, B.; Borges, J.G.; Oliveira, M.M.; Tomé, M.; Pereira, J.M.C. Modelling wildfire risk in pure and mixed forest stands in Portugal. *Allg. Forst Jagdztg.* **2012**, *183*, 238–248.
46. Cardil, A.; Molina, D.M.; Kobziar, L.N. Extreme temperature days and their potential impacts on southern Europe. *Nat. Hazards Earth Syst. Sci.* **2014**, *14*, 3005–3014. [CrossRef]
47. De Haan, J.; Icove, D.J. *Kirk's Fire Investigation*, 7th ed.; Pearson Education: New York, NY, USA, 2012.
48. Rachaniotis, N.P.; Pappis, C.P. Scheduling fire-fighting tasks using the concept of "deteriorating jobs". *Can. J. For. Res.* **2006**, *36*, 652–658. [CrossRef]
49. Haight, R.G.; Fried, J.S. Deploying wildland fire suppression resources with a scenario-based standard response model. *INFOR* **2007**, *45*, 31–39. [CrossRef]
50. Barreal, J.; Loureiro, M.L. Modelling spatial patterns and temporal trends of wildfires in Galicia (NW Spain). *For. Syst.* **2015**, *24*, e022.
51. Oliveira, S.; Pereira, J.M.C.; San-Miguel-Ayanz, J.; Lourenço, L. Exploring the spatial patterns of fire density in Southern Europe using Geographically Weighted Regression. *Appl. Geogr.* **2014**, *51*, 143–157. [CrossRef]
52. Rodrigues, M.; de la Riva, J. An insight into machine-learning algorithms to model human-caused wildfire occurrence. *Environ. Model. Softw.* **2014**, *57*, 192–201. [CrossRef]
53. Vasilakos, C.; Kalabokidis, K.; Hatzopoulos, J.; Matsinos, I. Identifying wildland fire ignition factors through sensitivity analysis of a neural network. *Nat. Hazards* **2009**, *50*, 125–143. [CrossRef]
54. Ruiz-Mirazo, J.; Martínez-Fernández, J.; Vega-García, C. Pastoral wildfires in the Mediterranean: Understanding their linkages to land cover patterns in managed landscapes. *J. Environ. Manag.* **2012**, *98*, 43–50. [CrossRef] [PubMed]
55. Vega-García, C.; Chuvieco, E. Applying local measures of spatial heterogeneity to Landsat-TM images for predicting wildfire occurrence in Mediterranean landscapes. *Landsc. Ecol.* **2006**, *21*, 595–605. [CrossRef]
56. Catry, F.X.; Rego, F.C.; Bação, F.L.; Moreira, F. Modeling and mapping wildfire ignition risk in Portugal. *Int. J. Wildland Fire* **2009**, *18*, 921–931. [CrossRef]
57. Gonzalez-Olabarria, J.R.; Mola-Yudego, B.; Pukkala, T.; Palahi, M. Using multiscale spatial analysis to assess fire ignition density in Catalonia, Spain. *Ann. For. Sci.* **2011**, *68*, 861–871. [CrossRef]
58. Martínez-Fernández, J.; Chuvieco, E.; Koutsias, N. Modelling long-term fire occurrence factors in Spain by accounting for local variations with geographically weighted regression. *Nat. Hazards Earth Syst. Sci.* **2013**, *13*, 311–327. [CrossRef]